FINE STRUCTURES IN THE ABSORPTION
SPECTRUM OF ALPHA-MnS

BY

Hiroo KOMURA*

SYNOPSIS

Absorption spectra in the visible region of α-MnS single crystals are investigated
at various temperatures. The ligand field theory is applied to interpret the entire spec-
trum, especially the fine structure which appears in a sharp and temperature-independent
band C ($^6A_{1g} \rightarrow [^4A_{1g}, \ ^4E_g]$). For all the absorption bands, certain experimental values
are determined; the location of peaks, the width at half-height, the absorption coefficient
and the oscillator strength. Calculation gives a good fit for the peak energy of observed
bands at liquid-helium temperature by adopting the covalency parameter $\varepsilon = 0.17$, the
Racah parameters $B = 808 \text{cm}^{-1}$, $C = 3751 \text{cm}^{-1}$ and the crystal field strength $Dq =
1025 \text{cm}^{-1}$. The introduction of covalent character, descent of the crystal field symmetry
and phonon participation are discussed in detail in order to interpret the causes of fine
structure of C band. Pure electronic transitions and a magnon sideband are found in
the fine structure of A band ($^6A_{1g} \rightarrow ^4T_{1g}$). These absorptions are identified by their
linewidths and relative intensities. The observed separation between a zero line and a
magnon sideband agrees with that theoretically calculated using the familiar spin wave
theory, which is briefly reviewed for a cubic antiferromagnet. Temperature dependence
of the separation is also measured and discussed to confirm the sideband being due to
a magnon. Other components of the A band are assigned as phonon sidebands.

Introduction

Spectroscopic research of antiferromagnetic materials has been developed rapidly,
since the discovery of the two-magnon absorption in FeF_2 by Halley and Silvera[1] and the
exciton-magnon absorption in MnF_2 by Greene et al.[2] As similar transitions were observed
in some particular compounds and an elaboration of the related theory was made, much
information has been accumulated on the association of an exciton with a magnon in antifer-
romagnets. These studies gave new aspects which had never been observed by means of
ordinary experimental methods used in the field of the conventional research on magnetism.
Up to the present, however, experimental studies were restricted to fluorides and oxides of
transition elements such as MnF_2 and $YCrO_3$.[3] No experimental studies on the exciton-
magnon transitions (magnon sidebands) have been reported in chalcogenides, although
other types of magneto-optical studies were actively made on rare earth chalcogenides and
chalcogenide spinels. The main purpose of the present paper is to report on the exciton-
magnon absorption in the selected antiferromagnetic chalcogenide, α-MnS. Two facts
should be mentioned as the reason for this selection: 1) α-MnS is the only one of the mono-
sulfides crystallizing in the relatively simple NaCl structure in which the transition metal

---

* On leave of absence from Faculty of Engineering, Shizuoka University, Hamamatsu.

ion is in the crystal field with the inversion symmetry. 2) Among transition metal chal-
cogenides, optical study in the paramagnetic state was made only about α-MnS.

Typically, magnon sidebands are observed in the crystals which have the inversion
symmetry. The intraionic d-d transitions are forbidden by Laporte's rule. Excitons are
excited by magnetic dipole transitions with very weak intensity. For an exciton-magnon
absorption, generation of an exciton should be accompanied by an absorption or an emission
of the magnon which has the same or opposite wave vector with reference to that of the
exciton. Magnon sidebands show relatively large intensity, since the electric dipole
transition is allowed by participation of an odd-mode magnon.

Historically, magneto-optical studies on antiferromagnets succeeded to the spectroscopic
research on paramagnetic crystals. Fine structures observed in the optical spectrum of a
paramagnetic crystal might be analyzed by the crystal field theory which assumed that lattice
vibrations and a magnetic interaction between magnetic ions could be ignored. Except
in a few crystals, however, the crystal field theory failed to elucidate the fine structures. The
situation forced one to recognize the importance of the magnetic interaction between ions.
Even in the paramagnetic region, few experiments on the optical properties of antiferro-
magnets have been made in manganese chalcogenides in comparison with halides. In the
first place, therefore, the optical spectrum of a manganese sulfide should be investigated in
the paramagnetic state.

The spectrum of the divalent manganese ion with $(3d)^5$ electronic configuration has
been one of the most fruitful sources of information about effects of coordinating ligands
on the central ion; the merit is based on the fact that the accidentally degenerate state $[^4A_{1g}(G),$
$^4E_g(G)]$ in the octahedral field formed by six ligands, splits under perturbation of covalent
bondings between the metal ion and ligands. Optical absorption spectra of manganese
hydrated salts were well understood using the molecular orbital description (ligand field
theory) in place of the simple crystal field theory (point charge model).[4] In MnF_2, the
point charge model could not account for the NMR spectrum.[5,6] Stout[7] gave the mixing
rate $\varepsilon = 0.064$ as the covalency parameter in order to interpret the optical absorption spectrum
of MnF_2. Fine structure of the absorption spectrum in $KMnF_3$ was explained by Stevenson
using covalency and the other effects.[8] In addition to the examples mentioned above,
introduction of some covalent character was required in various complexes and crystals,
in which case the situation was never understood without use of the ligand field theory.[9-11]

The only study of α-MnS reported seems to be the absorption spectrum in the visible
and near-infrared region investigated by Huffman and Wild.[12] In the visible region, they
reported that three absorption peaks A, B and C could be assigned as spin-forbidden transi-
tions from the ground state $^6A_{1g}(S)$ to the relevant excited states $^4T_{1g}$, $^4T_{2g}$ and $[^4A_{1g}, {}^4E_g]$
which originated from G level of $(3d)^5$ configuration in the free ion, respectively. The most
interesting band C (sharp and temperature-independent) has not been investigated in detail.
Covalent bondings should have an effect upon yielding a fine structure. Further, the band
will split when the crystal field symmetry is lowered or some other effects, such as a spin-
orbit interaction, exist. Also, a fine structure will be observed when participation of phonons
takes place. Another purpose of the present paper is to report on and interpret the fine
structure of C band by taking the above-mentioned effects into consideration, and to estimate
the crystal field and covalency parameters consistent with observed band positions. After
the discussion of optical properties in the paramagnetic state, the fine structure in the A
band tail is analyzed by taking account of the interaction between an exciton and a magnon
in the ordered state.

For preliminary knowledge, we must review previous studies on Neel temperature of

α-MnS. From magnetic susceptibility and specific heat measurements, α-MnS was known to show a transition to an antiferromagnetic state. Despite a number of different measurements, the Neel temperature was still uncertain. Anderson found two peaks at 139°K and 145°K of specific heat characteristics.[13] Several different values between 144°K and 167°K were reported from magnetic susceptibility measurements.[14-17] In this work, 147°K obtained most recently by Lines and Jones[18], is adopted as the Neel temperature.

Crystallographic data and constants with relation to the magnetic structure of α-MnS will be mentioned in the following chapters pertinent to the discussion of them.

Experiments

1   Synthesis of α-MnS powder

Three types of the crystal structure are known in MnS crystals. The α-MnS obtained most easily has a cubic NaCl structure with the distance of Mn-S bondings being 2.602Å.[19] The other crystal structures β and γ (zinc blende and wultzite structures) transform irreversibly into the stable α-type when they are heated.[20] One fortunate advantage of this sulfide is that it exists in a narrow range of stoichiometry near 1:1, whereas the oxygen content in transition metal oxides often varies over wide ranges.

MnS powder used in the crystal growth was prepared from a $MnCl_2 \cdot 4H_2O$ solution after Archer and Mittchel.[21] Manganese ions were precipitated from manganese chloride of reagent special grade when excess $(NH_4)_2S$ was poured into it. This pink solution containing the suspended precipitate was heated on a hot water bath, yielding the green α-MnS. The precipitate was washed several times with $(NH_4)_2S$ solutions with alcohol and with ether. After being dried in vacuo at room temperature, it was held at 1000°C in vacuo for several hours to vaporize excess sulfur and decompose polysulfides. Further, it was baked at 1150°C in the flow of dry H_2S for an hour to accomplish the last process. The assay of obtained powder samples was $Mn_{0.9993}S_{1.0007}$ containing very small amount of Fe and Cu.

2   Crystal growth

Because MnS has high melting temperature of about 1800°C and tends to decompose, growth methods starting from liquid phase are fairly troublesome.[22]* Hydrothermal growth is impractical because of extremely small solubility in ordinary solvents. Ordinary sublimation method is difficult because of the low sublimation rate below the softening point of quartz. The crystals used for the present experiment were grown by the chemical transport method. The chemical transportation has an advantage in that very thin crystals which cannot be obtained by polishing thick crystals, can be grown. Nitsche *et al.* succeeded in growing various chalcogenides by this method.[23] For the present experiment, almost the same method was taken to obtain single crystals. In the chemical transport method, highly volatile chemical intermidiates are vaporized at a lower temperature instead of vaporizing a solid directly at a high temperature. The back reaction of the resulting gas mixtures is made utilizing the temperature dependence of chemical equilibrium. Proper adjustment of the temperatures at the regions for vaporization and for crystal growth can make the departure from chemical equilibrium in the vicinity of growing seeds small enough to avoid polynucleation but large enough to make the seeds grow, *i.e.* proper supersaturation

---

* At Sony Corporation and the Institute for Solid State Physics (Tokyo University), single crystals with large sizes were grown by means of the melt-growing technique under high argon pressure to prevent decomposition.

can be maintained.   When iodine vapor is used as the transporter, equilibrium described by

$$MnS + I_2 \rightleftharpoons MnI_2 + 1/2 \cdot S_2$$
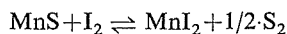
can be established in an evacuated tube placed in a furnace with an appropriate temperature gradient.   The reaction proceeds from left to right at the higher temperature and reverses at the lower temperature region.
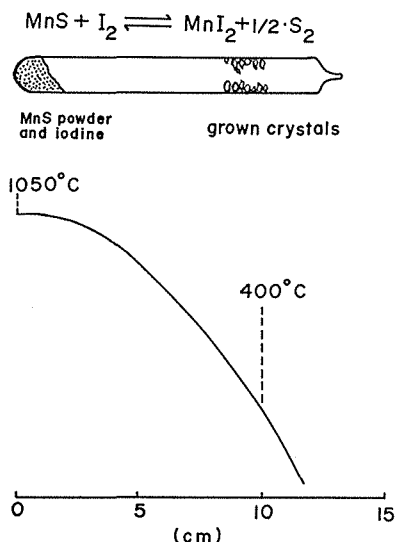

Fig. 1.   Schematic arrangement for growing α-MnS crystals.

Well baked MnS powder and iodine were introduced into quartz capsules evacuated to 10^{-6} Torr and sealed off.**   As shown in Fig. 1, they were left in a furnace with a strong temperature gradient for 96 hours.   The best condition to obtain the crystals suitable for optical measurements was when the high temperature region was kept at 1050–1100°C and the iodine concentration was in 5–10 mg per cubic centimeter of quartz capsules.   The temperature of the furnace was controlled so that the fluctuation might be within 0.2°C throughout the crystal growth.   This severe condition was necessary to maintain a proper supersaturation condition.   Crystals were easy to grow in the 450–500°C region of capsules. To avoid new nucleation on the surfaces of crystals during cooling process, the capsules were removed without turning off the furnace and immediately immersed into water.   This treatment ceases the reaction quickly and assures smooth faces on as-grown crystals.   Some crystals were thin platelets (from a few to 500 micron thick) with (111) large faces, which were identified by X-ray Laue patterns.   The surface area of some platelets was large enough to make optical measurements.

3   Absorption measurements

Absorption measurements are rather easy on the broad bands appearing in the visible region and the fine structure of C band.   On the other hand, a different complex procedure must be carried out on the fine structure of A band.   The reason for the difference is the

---

** Researchers of Broadcasting Research Laboratories of NHK obtained single crystals using Mn and S as starting materials.

extremely sharp and weak absorption of each component in the latter.

The entire spectrum in 3400–7000Å wavelength region was recorded with a Cary model 14R spectrometer at liquid-helium, liquid-nitrogen and room temperatures. The incident light was always directed perpendicular to the (111) faces. The apparatus was set so that its resolution was better than 2Å in 4400–7000Å, while the resolution decreased considerably in 3400–4400Å owing to the strong absorption edge located at 4400A (at room temperature). This absorption edge was accounted for as the charge transfer absorption from sulfur to divalent manganese ion.[12] As the wavelength is scanned, the instrument automatically corrects spectral variation of intensity of the incident beam and plots the absorbance $\ln(I_0/I)$ versus the wavelength, where I_0 and I correspond to the output intensity of the reference and sample beam, respectively. Selected crystals were mounted over suitably drilled holes in tin plates. Pairs of identical plates were always prepared. The one plate without the crystal, placed in the reference beam, could be used as a reference for zero absorption. Various grade mesh filters were put in the reference beam for adjustment of zero absorption when the optical dewar system for low temperature measurements was placed in the sample beam. Numerous specimens with a wide range of thickness were employed to measure exact absorption coefficients.

The fine structure of A band at 4.2–50°K was photographed using Kodak 103–F infrared plates through a Baush-Lomb dual grating spectrometer giving dispersion of 8Å/mm or 4Å/mm on photographic plates. The slit width was fixed at 50 microns throughout the experiment. The resolution of the apparatus was better than 0.5Å. As the light source, a 20W tungsten lamp with ribbon type filament, was employed. Photoelectric detection is apt to fail to attain the observation of extremely sharp and weak exciton lines. Unless the paticular detection technique such as a photon counting method is employed, those
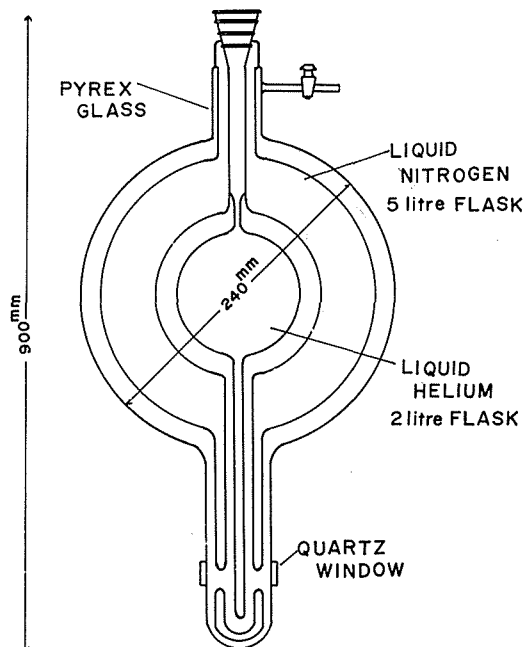

Fig. 2.   A dual pyrex glass cryostat. Its peculiar shape was designed not to give rise to rapid temperature increase of specimens.

lines would disappear in noises, because incident light decreases considerably through a narrow slit of a spectrometer set for good resolution. Thus, photographic detection was adopted in place of photoelectric detection. The spectroscopic grade plate has the resolution of 56 lines/mm which is able to discriminate two lines separated by 0.14A for the dispersion of 8A/mm. In order to obtain good results, great care was taken to select the crystals with thickness suited for the optical study in view of the fact that the intensity of both of exciton lines and sidebands is considerably weaker than the background absorption. Good results were obtained for the crystals with thickness of 100 to 500 microns.

The measurement above 4.2 °K was made after liquid helium had been evaporated. A double cryostat used is illustrated in Fig. 2. Its peculiar shape was designed not to bring about rapid temperature increase of specimens. The crystal temperature rises gradually up to 50 °K for about 90 minutes, the temperature rise rate being 0.01 °K per second. Exposure times were between 10 and 20 seconds, by taking into consideration the absolute intensity relative to the background fog. Short exposure time enabled one to avoid appreciable temperature change during each exposure. Temperature of a specimen was monitored by a bolometer which was rested on the crystal-mount.

By the employment of photographic detection, exciton lines and a magnon sideband could be observed. But their profiles were not obtained in the form of the exact shape function, because their intensities, relative to the background fog, were very weak and phonon sidebands prevented determination of the shape of the magnon sideband.

Results

Observed spectral lines and bands in the visible and near-ultraviolet regions are listed in Table I, together with the assignment and some relevant values. Five absorption bands were found and named A, B, C, D and E from the lower to the higher energy side. Three absorption bands A, B, C in the visible region are shown in Fig. 3. Except for the C band, all the absorption bands were fairly broad. In contrast to the relatively temperature-independent band C, A and B bands showed large shifts to the higher energy side when temperature was decreased. Absorption coefficients were obtained only by dividing the recorded optical density by thickness of the specimens. The thickness of very thin platelets was measured exactly from interference fringes as shown in Fig. 4. Those fringes arise from multiple reflections within a crystal throughout the transparent region. Thickness was obtained by counting the number of fringes Δm between $\lambda_1 = 1.4\mu$ and $\lambda_2 = 1.6\mu$ from the equation $d = \Delta m/2n \cdot (1/\lambda_1 - 1/\lambda_2)$. The index of refraction ($n = 2.695$) which had been measured at 1.5μ by Huffman and Wild[12] was adopted. The oscillator strength was calculated from the expression

$$f = \frac{[\int \alpha(\nu)d\nu]_{\text{observed}}}{[Ne^2/1000c^2 C_0 m]} = 1.09 \times 10^{-10} \int_{-\infty}^{\infty} \alpha(\nu)d\nu,$$

where e and m are the charge and mass of an electron, c and $\bar{\nu}$ are the velocity and wave number of light, N is Avogadro's number, C_0 is the molecular concentration per litre of MnS and α is the absorption coefficient. With the aid of the following expression, the integral was calculated from the absorption coefficient at the peak ($\bar{\nu}_0$) and the half-maximum width ΔW assuming a Gaussian shape: $f = 1.09 \times 10^{-10} \cdot \alpha(\nu_0) \cdot \Delta W(\pi/\ln 2)/2$.

The fine structure was observed in C band when a specimen was cooled to a temperature below 77 °K. The typical feature of C band at different temperatures is shown in Fig. 5. At liquid-helium temperature, five peaks were found and named $C1$–$C5$,
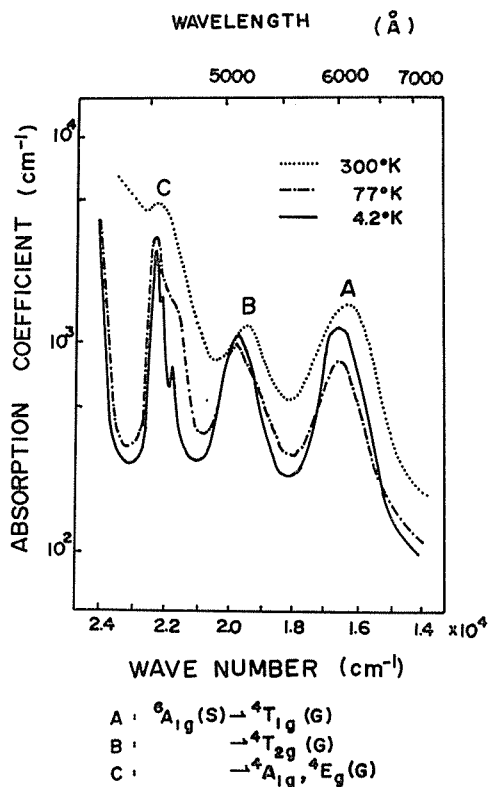
WAVELENGTH (Å)

Fig. 3. Absorption spectra of α-MnS in the visible region.
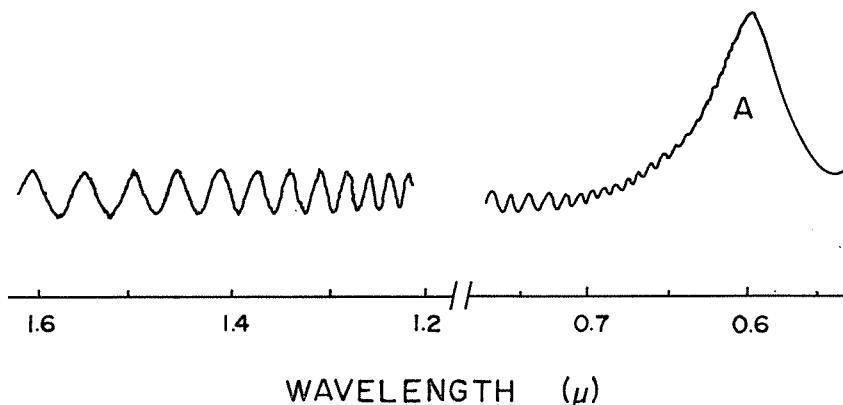
Fig. 4. Interference fringes appearing in the absorption spectrum. Thickness of thin
specimens was obtained by counting the number of fringes between 1.4μ and 1.6μ.

Figure 6(a) shows the structure in the absorption tail of A band at liquid-helium
temperature. Lines were named $A1$–$A5$, from the lower to the higher energy side. It
should be noted that two extremely sharp and weak lines $A1$, $A2$ (their widths were less than
2 cm^{-1}) emerged in the lower energy side and $A3$, $A4$ and $A5$ had much more intense absorp-
tion than $A1$ and $A2$. Each component in the structure of A band tail is illustrated in Fig.
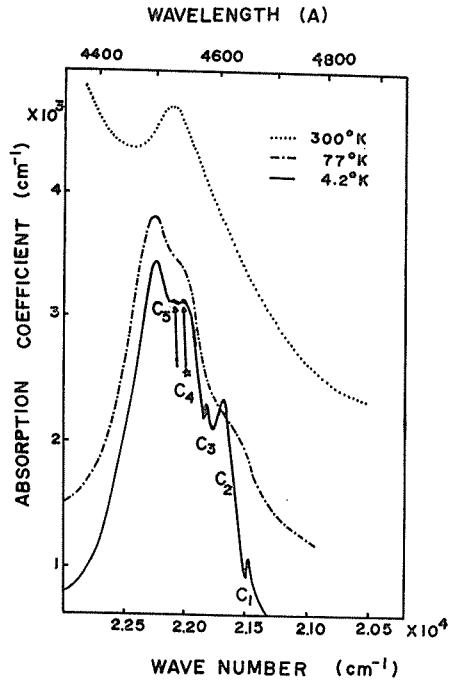
WAVELENGTH (A)

Fig. 5. Fine structure of C band. The arrows with and without an asterisk indicate the positions of phonon-assisted transitions $^6A_{1g} \rightarrow {}^4E_g(1) + 2\bar{\nu}_{L.O.}$ and $^4E_g(1) + 2\bar{\nu}_{T.O.}$, respectively.
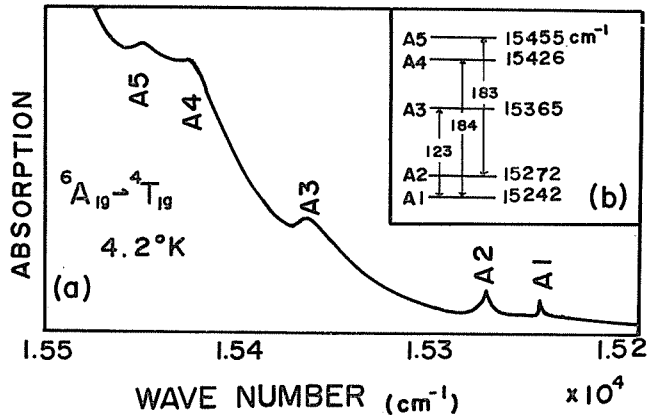

Fig. 6. (a) Structure in the tail of A band recorded by a microphotometer. (b) Each component of the structure is described in terms of an energy level scheme.

6(b). The separation between $A1$ and $A3$ was different from the two nearly equal separations of $A1$–$A4$ and $A2$–$A5$. In Fig. 7, temperature dependence of the spacing between $A1$ and $A3$ is shown together with that of the zero-field Mn^{55} NMR frequency $\nu^{55}(T)$ in the antiferromagnetic state.[18] The separation at 0°K extrapolated from empirical values at other temperatures was found to be 127 cm^{-1}. Since each component of the structure diffused
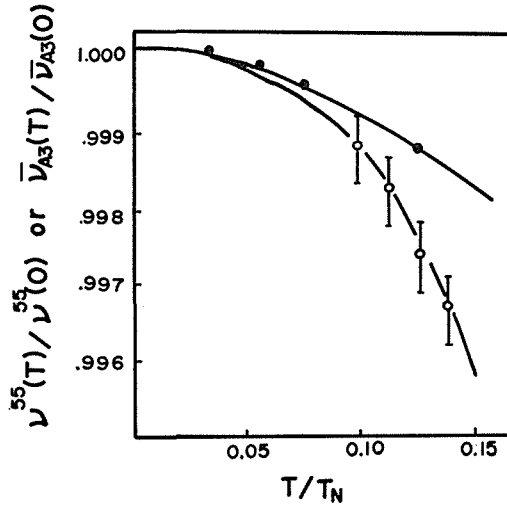
Fig. 7.   Normalized temperature dependence of the magnon frequency $\omega_M(T)$ and the Mn[55] NMR frequency ν^{55} after Lines and Jones.   The solid and open circles show the former and the latter, respectively.   The wave number of the sideband is denoted by $\bar{\nu}_{A3}(T)$.

above 30°K presumably due to thermal vibration, the separation could not be measured accurately.   The assignment of the structure is discussed in the next chapter.

Discussion

This chapter is divided into two sections.   In the first section, the whole spectrum and the fine structure of C band are discussed using the modified crystal field theory.   We have no regard for the effect of antiferromagnetic ordering.   In the second section, the fine structure of A band tail is discussed in detail and assigned as a group of pure exciton absorptions and their sidebands.

1   Absorption spectrum of paramagnetic α-MnS

As summarized in Table I, measured values of the oscillator strength of all the bands are too large to be accounted for as the absorption being due to forbidden d-d transitions. Electric dipole transitions between the ground state and the excited states are highly forbidden because of the same parity and different spin multiplicity of them.   It should be taken into consideration that the descent of a crystal field symmetry and/or the cooperation of phonons with appropriate modes, relax Laporte's rule in the field of the inversion symmetry.   On the other hand, the transition from sextet to quartet becomes possible through the spin-orbit interaction.   Koide and Pryce showed that the introduction of the intermediate state $^4T_{1g}(G)$ couples the ground state with excited states, since ^6S state couples only with ^4P through the spin-orbit interaction and $^4T_{1g}(P)$ is mixed in $^4T_{1g}(G)$.[4]   Such a mechanism may loosen the prohibition of d-d transitions.

1.1   Assignment of bands in the visible region

Three bands A, B, C are the d-d transitions from sextet to relevant excited states.   Apart from the confirmed bands, the assignment of D and E bands appearing in the 4400A strong

Table I. Absorption spectrum of α-MnS. The sign † indicates the calculated positions of absorption peaks. In the last two rows D and E at 4.2°K, the band positions calculated on the assumption peaks. In the last two rows D and E at 4.2°K, the band positions calculated on the assumption that the transitions occur from $^6A_{1g}(S)$ to $^4T_{2g}(D)$ and $^4E_g(D)$, are given in parentheses, respectively. The misfit between these transitions and D, E suggests that the two bands obtained experimentally do not result from any d-d transitions in a manganese ion.

Absorption peak	Wavelength Å	Wave number (cm⁻¹)	Width at half-height (cm⁻¹)	Oscillator strength	Transition $^6A_{1g}\rightarrow$	Absorption coefficient (max.) (cm⁻¹)	Remarks
at 4.2°K							
A	6010	16640 †16391	~1400	1.7×10^{-4}	$^4T_{1g}$	1.03×10^3	
B	5040	19840 †20111	~1200	1.5	$^4T_{2g}$	1.06	
C_1	4664	21440	90	0.1	$^4E_g(2)$	0.90	
C_2	4617	21659 †21649	180	0.5	$^4E_g(1)$	2.18	
C_3	4532	21825			$^4E_g(1)+\bar{\nu}_{\text{T.O.}}$	2.18	
C_4	4540	22030			$\begin{cases}^4E_g(1)\times\bar{\nu}_{\text{L.O.}} \\ ^4E_g(1)+2\bar{\nu}_{\text{T.O.}}\end{cases}$	2.98	shoulder
C_5	4490	22270 †22273	400	1.5	$^4A_{1g}$	3.30	
D	4050	24691		($^4T_{2g}(D)$:†28035)			broad
E	3650	27397		($^4E_g(D)$: †28367)			broad
at 77°K							
A	6010	16640	~1500	1.8		1.06	
B	5040	19840	~1300	1.8		1.21	
C_2	4625	21620					shoulder
C_4	4550	21980	over-all 520				shoulder
C_5	4503	22210				3.60	
at 300°K							
A	6070	16470	~1500	2.3		1.32	broad
B	5150	19420	~1400	2.0		1.26	broad
C	4525	22100	880	4.5		4.50	sharp

absorption edge comes into question. One can suspect that the transitions occur from the ground state to excited states $^4T_{2g}$ and ^4E_g which originate from free D level. It will be seen later, however, that the calculated energies of $^4T_{2g}(D)$ and $^4E_g(D)$ terms deviate largely from experimental values of D and E. The two bands may be due to a structure which is responsible for a charge transfer absorption located in the strong absorption edge around 4400Å.

1.2 Fine structure of C band

Our assignment of five lines in the fine structure were made by inspection of spectral features shown in Table I and Fig. 5. Three components $C5$, $C2$ and $C1$ are due to the transitions to $^4A_{1g}$, $^4E_g(1)$ and $^4E_g(2)$, respectively, where $^4E_g(1)$ and $^4E_g(2)$ express two sublevels from ^4E_g split by distorted field in the crystal. The splitting into $C2$ and $C5$ is due to the partial covalency in the Mn-S bonding. The other peaks are phonon-assisted transitions of $C2$. That is, $C3$ is accompanied by one transverse-optical (T.O.) phonon emission and $C4$ consists of two absorption peaks; a transition coupled with one longitudinal-

optical (L.O.) phonon emission and the other two-T.O.-phonon emission. The justification of the assignment is discussed as follows.

Certain mechanisms can be considered as the source of splitting of the degenerate state [$^4A_{1g}$, ^4E_g]. In the initial and final states of the transition responsible for C band, the effect of the spin-orbit interaction should be ruled out, since it would give much smaller splitting ($\sim$10 cm^{-1}) of the second order. Similarly, the first order spin-spin interaction is not effective for the splitting.[4] For the explanation of the observed structure, we should consider the splitting to be due to the covalency, the distorted field and the vibrations coupled with electronic transitions.

A larger covalency can be expected in sulfides than in halides, since the electron negativity difference in the former, is much larger than in the latter. Indeed, the value of the effective ionic charge of the Mn^{2+} ion derived from infrared reflectance data suggests considerable covalency in MnS.[12] Lee obtained f_s=0.915% as the effective fraction of valence electrons by the NMR experiment of S^{33} in the paramagnetic α-MnS.[24] The calculation by Koide and Pryce[4] which took covalency into consideration showed that the curves of energy levels $^4A_{1g}$ and ^4E_g as functions of the covalency parameter intersect each other at a certain value of the parameter, i.e. ^4E_g is located above $^4A_{1g}$ for the smaller degree of covalency and vice versa for the larger one (Fig. 8).
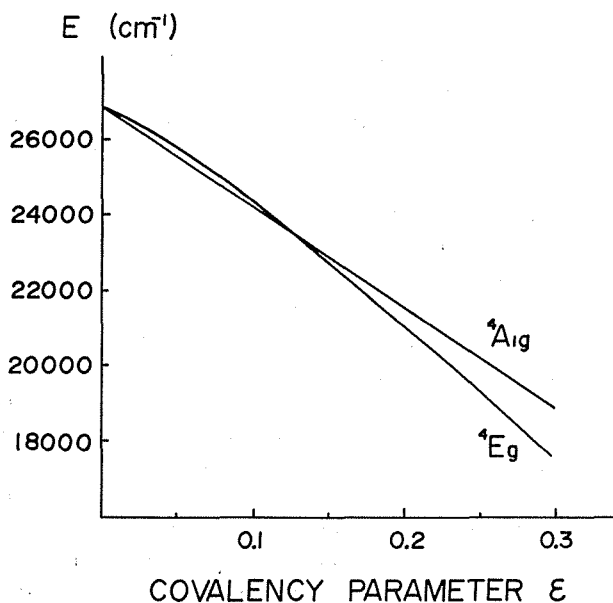

Fig. 8. Variation of the energy levels $^4A_{1g}$, ^4E_g as functions of covalency parameter ε.

Next, consider the effect of the distorted field in α-MnS. It lowers the symmetry of the crystal field from O_h to a certain symmetry species. The state $^4A_{1g}$ is not influenced by the effect, while ^4E_g decomposes further into two sublevels. One is located at the same position as in the absence of the distorted field and the other shifts to the lower energy side.[4] We call the former $^4E_g(1)$ and the latter $^4E_g(2)$. The reduction of the symmetry comes from two sources, although at this stage of our experiments we cannot decide which is more dominant. A lattice distortion by magnetic ordering causes the descent of the crystal field

symmetry.   In addition to an isotropic contraction along all cube edges, a lattice deformation along [111] axis has been reported in MnO and NiO which have the same magnetic structure as antiferromagnetic α-MnS.[25,26] In α-MnS rather small lattice distortion was measured.[18] The other origin which gives rise to the descent of the symmetry is an impurity incorporation. In the specimens grown by the chemical transport method, the distorted field is easily supposed to exist, for the iodine atoms used as the transporter diffuse into a crystal during the growth of single crystals.   The iodine content amounts to 10^{-2} weight per cent in the case of CdS.[23] Whether they migrate to substitutional or interstitial sites, the introduction of iodine ions decreases a crystal field symmetry.

It may be assumed that the covalency is so large as to raise $^4A_{1g}$ to a higher energy than ^4E_g.   This assumption is supported by the calculation of term energies discussed later.

The difference between $C2$ and $C3$ agrees with the T.O. phonon frequency $\nu_{T.O.} = 185 cm^{-1}$ obtained from an infrared reflectance within the experimental error.[12] Two absorption peaks which compose the $C4$ shoulder are of the transitions to $^4E_g(1)$ level coupled with the L.O. phonon ($\nu_{L.O.} = 320\ cm^{-1}$) and two T.O. phonons.   The shoulder $C4$ is relatively broad owing to the coexistence of two phonon-assisted transitions.   The positions of these transitions are indicated by arrows in Fig. 5.   It is reasonable that the transitions accompanied by the phonon emission may overwhelm those by the phonon absorption at low temperature.

1.3   Estimation of covalency and crystal field parameters

In the free ion the separation in energy among the levels derived from $(3d)^5$ configuration arises from the Coulomb and exchange integrals describing the electrostatic repulsion between the electrons.   These integrals may be expressed in terms of the Racah parameters[27-29], which in turn may be written with the Condon-Slater integrals[30], namely $B = F_2 - 5F_4$ and $C = 35F_4$.   Since in α-MnS each Mn^{2+} ion is surrounded by six sulfur ions at equal distance, one expects that the change in the location of electronic energy levels in passing from the free ion to the crystal, may in the first approximation be described with the perturbation of the free ion levels by a ligand field of octahedral symmetry.   In the O_h field the strength of the ligand field can be specified by a single parameter Dq, from which it is possible to calculate the positions of energy levels in the crystal.   Tanabe and Sugano[31-33] and Orgel[34-36] calculated the expected energy level patterns for ions containing an incomplete shell of d electrons.   In their energy level scheme, the ligands were regarded only as point charges which give rise to O_h field.   The overlap between the electron clouds of the Mn^{2+} and the S^{2-} ions, i.e. the covalent bonding, must be considered.   The screening by the electrons from the sulfur ions causes the radial distribution of charge in e_g orbitals of the metal ion to move away from the nucleus.   But little effect is expected on t_{2g} orbitals. Taking into account the covalent character as the covalency parameter ε, Koide and Pryce calculated the energy matrices for $^4E_g(G)$ and $^4A_{1g}(G)$ for the interpretation of their experiment on the absorption spectrum of manganese hydrated salts.[4] In their formalism, the amplitude of each e– eigenfunction is diminished by the factor $(1-\varepsilon)^{1/2}$.   For the discussion of absorption spectrum of MnF_2, Stout developed the calculation to all energy matrices relevant to $(3d)^5$ configuration containing the covalency parameter.

Taking the partial covalency of the Mn-S bonding into consideration, the values of the Racah parameters B, C and crystal field strength Dq were determined so as to fit the positions of four observed bands and two lines $C2$, $C5$.   Each term energy was calculated using the secular equations of energy matrices for relevant terms which contain the covalency parameter ε.   After the work by Stout, energy matrices which are necessary for the present work are shown in Table II.   By changing ε step by step from zero to 0.30, a wide range of B, C and Dq was examined with an electronic computer so as to obtain the best fit of the

Table II. Energy matrices of some terms of the Mn^{2+} ion in the crystal after Stout. The origin of energy is the $^6A_{1g}(S)$ ground state.

$^6A_{1g}(S)$	0		
$^4A_{1g}(G)$	$(10B+5C)(1-\varepsilon)$		
$^4E_g(D, G)$	$13B+5C$ $-\varepsilon(4B+2C)$	$2\sqrt{3}\,B(1-\varepsilon)$	
		$14B+5C$ $-\varepsilon(22B+7C)$	
$^4T_{1g}(P, F, G)$	$10B+6C-10Dq$ $-\varepsilon(18B+C)$	$3\sqrt{2}B(2-\varepsilon)/2$	$C(1-\varepsilon)$
		$19B+7C$ $-2\varepsilon(2B+C)$	$3\sqrt{2}\,B(2-\varepsilon)/2$
			$10B+6C+10Dq$ $-10\varepsilon C$
$^4T_{2g}(F, D, G)$	$18B+6C-10Dq$ $-\varepsilon(26B+C)$	$\sqrt{6}\,B(2-\varepsilon)/2$	$(4B+C)(1-\varepsilon)$
		$13B+5C$ $-2\varepsilon(2B+C)$	$-\sqrt{6}\,B(2-\varepsilon)/2$
			$18B+6C+10Dq$ $-\varepsilon(8B+10C)$

values of them for the observed positions of absorption peaks. We obtained reasonable values; $\varepsilon=0.17$, $B=808$ cm^{-1}, $C=3751$ cm^{-1} and $Dq=1025$ cm^{-1}.

The rather large value of ε should be compared with 0.064 in MnF_2, 0.03 or 0.13 in MnCl/ and 0.05 or 0.15 in $MnBr_2$.[7.37-39]* Trials to seek the set of reasonable values of the parameters always miscarried for the smaller ε for which $^4A_{1g}$ was located below ^4E_g. It is well known that 1) $\gamma=C/B$, is nearly the same for almost all elements, taking a value 4 to 5.[32] 2) the magnitude of the interelectronic repulsion parameters B and C would be reduced to some extent in many complexes and molecules unless the covalency parameter is taken into consideration.[40-42] The reduction comes from the partial covalency of the bondings between a central ion and ligands. In our case of the crystal field, nearly the same values as in a free ion were obtained, since such a reduction of the magnitude was transferred to the large value of ε. Thus, we obtained a reasonable value 4.64 as the γ value.

The rather large crystal field strength Dq never spoils the level diagram used in the interpretation of the absorption spectrum. When the octahedral crystal field becomes much stronger, $^2T_{2g}(I)$ with the $(t_{2g})^5$ configuration eventually becomes the ground state in place of $^6A_{1g}(S)$ with the $(t_{2g})^3(e_g)^2$ one. Then we gain 20 Dq by two electrons transferring from the e_g shell to the t_{2g} shell at the expense of $15F_2+275F_4$ in promotional energy. The condition for $^2T_{2g}(I)$ to be the ground state can be expressed as $20Dq-(15F_2+275F_4)>0Dq$ where $0Dq$ is the energy of $^6A_{1g}(S)$ state.[43] The calculated values of Dq is the appropriate one to our case.

---

* Two different values of the covalency parameter have been obtained for $MnCl_2$ and $MnBr_2$. Stout took the values of the free Mn^{2+} ion as those of B, C, whereas Pappalardo thought of ε, B, C and Dq as adjustable parameters. See reference 37–39) for detailed discussions.

2   The absorption spectrum of antiferromagnetic α-MnS

The theoretical study of magnon sidebands in cubic antiferromagnetic manganese compounds involves detailed and complicated calculations: the location of magnon sidebands measured from the exciton absorption line can be estimated after the construction of Brillouin zone and the bulky calculation of magnon dispersion relation and density of states. In the subsections 2.1–2.3, the spin wave theory will be briefly reviewed on cubic antiferromagnets in order to facilitate the subsequent calculation.   The enumeration of the location of magnon sidebands is carried out by taking into account the observed values of parameters. In the last two subsections, experimental results are discussed on the assignment of the structure in the A band tail and the temperature effect of magnon sidebands.   It was found very recently that Motizuki and Harada made a more detailed investigation on magnon sidebands in MnO and MnS.[44]   Their results of numerical calculations cannot be adopted directly for our experimental results, because parameters used by them are slightly different from observed values for the sake of theoretical manifestation.

2.1   Spin wave Hamiltonian and magnon dispersion relation

The α-MnS has the antiferromagnetic ordering denoted as an fcc-2-type ordering (Fig. 9).[36]   Calculation of the magnon frequency in terms of exchange and anisotropy fields in α-MnS is more complicated than in MnF_2-type antiferromagnets, since a half of twelve nearest neighbors (nn) is located on the same sublattice as the central spin and the other half on the different sublattice.   Six next nearest neighbors (nnn) have antiparallel spins with the central spin.   For this ordering, an indirect exchange mechanism should be rather favorable since the next nearest neighbor and an intermidiate anion lie along a straight line.   The spin wave Hamiltonian consists of the exchange interaction between nn's and between nnn's and anisotropy energies.   In α-MnS the spin direction was found to be in ferromagnetic sheets rather than along cube edges.[25]   There exist 'out-of-plane' and 'in-plane' anisotropy energies.   The former constrains the spins to lie in (111) plane.   The latter fixes the spins to certain preferred orientations within easy planes.   The small contribution from the 'in-plane' anisotropy energy (0.001 °K) can be neglected in comparison with the other interactions contained in the spin wave Hamiltonian.
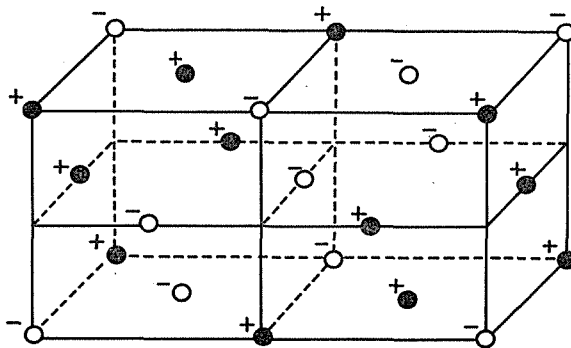

Fig. 9.   An fcc–2–type ordering. The signs+and−mean 'up' and 'down' spins, respectively.

The Hamiltonian can be written as

$$H = \Sigma_{i,j} J(R_{ij}) S_i \cdot S_j + D \Sigma_i S_{i(111)}^2 \ .$$

(1)

The first term involves nn and nnn exchange interactions; the second coresponds to 'out-of-plane' anisotropy energy. The exchange integral in real space is denoted as $J(R_{ij})$. The set of i,j runs over all parallel and antiparallel nn spins S_j and all nnn spins S_j of the central spin S_i. The parameter D is related to the anisotropy energy K by $D=3K/2NS^2$ where N is the number of spins in the system. The anisotropy energy gives an effective field of $-2DS_{[111]}$ in the [111] direction for each spin.

For the following calculation, we should review helical spin ordering in magnetic crystals. The term is applied to the spin ordering in which spins in a plane of a crystal point in the same direction and this direction turns from one plane to the next by an angle proper to each helical magnet. The spin arrangement in α-MnS can be regarded as a helical magnet in which spins rotate by π when they are transferred from a (111) plane to the adjacent plane. On the theory of helical magnetism, we can refer to the detailed discussion by Nagamiya.[45]

In terms of the Holstein-Primakoff formalism for the spin wave, (1) can be diagonalized and the spin wave frequency is obtained as follows:[45]

$$\hbar\omega_k = 2[(A_k+B_k)(A_k-B_k)]^{1/2} \qquad (2)$$

where

$$A_k = [D-J(\mathbf{k})+2J(\mathbf{Q})-J(\mathbf{k+Q})]S/2 , \qquad (3)$$

$$B_k = [J(\mathbf{k})-J(\mathbf{k+Q})-D]S/2 . \qquad (4)$$

In the above expressions, the exchange integral in real space $J(\mathbf{R}_{ij})$ is transferred into $J(\mathbf{k})$ in k-space by the Fourier transformation:

$$J(\mathbf{k}) = \Sigma_i J(\mathbf{R}_{ij}) \exp(i\mathbf{kR}_{ij}) . \qquad (5)$$

The wave vector $\mathbf{Q} = [\pi, \pi, \pi]/a$ (a: lattice constant) describes the spin arrangement in the fcc-2-type ordering and $J(\mathbf{k})$ has the highest maximum for the wave vector.

2.2 Magnon dispersion relation along the paticular lines of the Brillouin zone

Numerical calculation on the magnon dispersion relation can be carried out using the expression (2)–(5). Then $J(\mathbf{k})$ must be transferred into the form pertinent to an fcc lattice. From the formula (5), $J(\mathbf{k})$, $J(\mathbf{Q})$ and $J(\mathbf{k+Q})$ are written as follows in terms of the exchange integrals J_1 between nn spins and J_2 between nnn spins;

$$J(\mathbf{k}) = 4J_1[\cos(k_xa/2)\cos(k_ya/2)]^\dagger + 2J_2[\cos(ka)]^\dagger , \qquad (6)$$

$$J(\mathbf{Q}) = -6J_2 , \qquad (7)$$

$$J(\mathbf{k+Q}) = 4J_1[\sin(k_xa/2)\sin(k_ya/2)]^\dagger - 2J_2[\cos(ka)]^\dagger , \qquad (8)$$

where $\dagger$ means the sum of the permutation about x,y,z.

For an fcc lattice, the Brillouin zone (BZ) is a truncated octahedron. Five critical points are of unusual interest; X, K, L, W and U. Together with the BZ, the magnon dispersion relation (2) was numerically calculated and illustrated in Fig. 10 only along the directions Δ, Σ, Λ using the values of J_1, J_2 and D obtained by Lines and Jones.[18] In their work, a zero-point spin deviation of 3.2 % from the $S=5/2$ Neel state also was estimated in order to account for the temperature dependence of the sublattice magnetization. Therefore, the value of $S=2.42$ was used as S in (3), (4) in calculation of magnon frequency. Except for the Δ direction, the other two dispersions have asymmetric features, which come from the asymmetric spin arrangement in the fcc-2-type ordering.

2.3 Density of states and the location of magnon sidebands.

In this paper, we are not concerned with the exact shapes of magnon sidebands but only with the location of them. For our purpose, it is sufficient to calculate only the density of states. The observed sidebands move from pure electronic transitions by the magnon
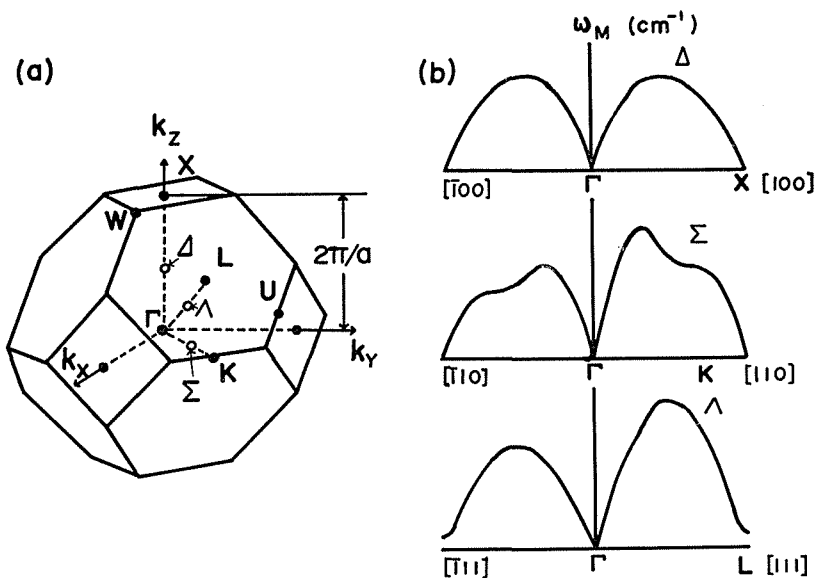
(a)

(b)

Fig. 10. First Brillouin zone of an fcc lattice and magnon dispersion curves along the
paticular lines. The enumeration of the magnon frequency was made using $J_1=$
$-3.5\,^\circ K$, $J_2=6.25\,^\circ K$, $D=0.28\,^\circ K$ and $S=2.42$.
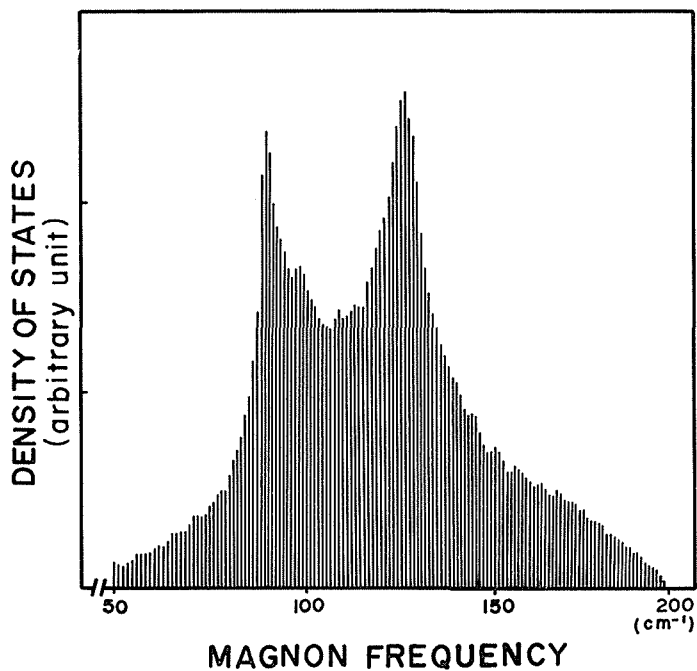

MAGNON FREQUENCY

Fig. 11. Density of states versus magnon frequency. The histgram was obtained from
computed magnon frequencies for 128,000 wave vectors.

frequency corresponding to the peak of the density of states. By counting the number of wave vectors which give the same magnon frequency, one can obtain the histogram of the density of states illustrated in Fig. 11. Magnon frequencies were calculated with the aid of an electric computer for the 128,000 wave vectors distributed on a cubic net through the volume element of the first BZ. Two peaks come out in the density of states. As shown in the last subsection, the dispersion curve along Σ direction ([110]) has a constant frequency region. The higher energy peak in the density of states comes from the flat part in [110] direction. The other peak originates from the contribution of the flat parts in the other Σ directions [110], [101] and [011]. The magnon sideband responsible for the higher energy peak should be observed in an experiment. No contribution is expected from the lower energy peak, for the intensity of magnon sidebands is absolutely zero because transition probability at the magnon frequency vanishes.[44]

From the above discussion, it is expected that pure electronic absorptions have each magnon sideband separated by 128 cm^{-1} on the higher and lower energy sides corresponding to magnon emission and absorption processes.

2.4 Identification of the structure in the A band tail.

From the standpoint of the line width and the spacing between its components, the observed structure is essentially different from that of the C band previously assigned in terms of covalency and some other effects. Sharp lines $A1$, $A2$ are pure electronic transitions (the so-called zero magnon lines), whereas $A3$ is the magnon sideband of $A1$. From the experimental results described previously, the assignment can be made mainly on the basis of the following facts: 1) the sideband $A3$ has a much more intense integrated absorption than zero lines 2) the separation between $A1$ and $A3$ at 0°K (127 cm^{-1}) agrees with the magnon frequency 128 cm^{-1} theoretically calculated 3) Temperature dependence of the separation between $A1$ and $A3$, which will be mentioned in the next subsection, confirms that $A3$ is the magnon sideband of $A1$. The complete agreement stated in 2) as well as the temperature effect on the magnon sideband affords the conclusive evidence of simultaneous excitation of an exciton and a magnon. The possibility of the observed sideband being vibronic is ruled out, because phonon wave numbers are much larger than the observed separation. Other components $A4$ and $A5$ may be assigned as phonon sidebands: the separation $A1$–$A4$ and $A2$–$A5$ coincides with the wave number of the transverse-optical phonon 185 cm^{-1}.[12]

The reason why two zero lines were observed and the magnon sideband associated with $A2$ was not observed is still obscure. The cause of the former is presumed to be the small lattice distortion along the [111] axis by magnetic ordering. It lowers the crystal field symmetry from the octahedral to the trigonal field, as mentioned in section 1. The orbital degeneracy is removed by reduction in symmetry. The state $^4T_{1g}$ decomposes into a non-degenerate $^4A_{2g}$ and a twofold-degenerate ^4E_g state.[40] The magnon sideband for $A2$ may be buried in the tail of the phonon sideband $A4$.

2.5 Temperature dependence of magnon sideband

Observed temperature dependence of the separation between a zero line and a sideband is used to confirm the sideband being due to a magnon. As the temperature increases, magnon sidebands shift towards a zero line according to the decrease of sublattice magnetization. The shift of phonon sidebands cannot be expected, because in a small range of temperature increase the expansion of the lattice can be ignored.

The magnon frequency should have the similar temperature dependence as the NMR frequency shift which reflects that of the sublattice magnetization. The shift in both the NMR experiment and the present study of the magnon sideband is much less than in MnF_2.

Weaker temperature dependence of magnon frequency was observed in comparison with the NMR frequency shift. Such characteristics have been reported in many cases[47,48] since the short range ordering is considered to be responsible for the optical effects. Temperature dependence of magnon frequency behaves as if there were the effective T_N above the real T_N at the long range antiferromagnetic ordering vanished.

Concluding Remarks

The results of this work are summarized as follows:

1) The most important result is that an exciton-magnon absorption was observed in α-MnS. It is the first time that a magnon sideband has been observed in a transition metal chalcogenide. The observed magnon sideband was confirmed with the aid of the theoretical study and the observation of its temperature effect.

2) In relation to 1), the fine structure of A band was assigned as a group of exciton lines and their sidebands due to a magnon and a phonon.

3) Five absorption bands were observed in the visible region and interpreted in terms of the modified crystal field theory. In particular, the fine structure of C band was investigated in detail.

4) When the calculation of the term energies responsible for optical transitions was carried out so that observed band positions could be explained, the results gave the reasonable values of parameters γ and Dq. Estimation was also made for covalency and the Racah parameters ε, B, C consistent with the experimental data.

In view of the fact that our main purpose to obtain the physical insight of experimental features was attained, the results of the present study on MnS are considered to be satisfactory. Exact line profile of the magnon sideband, however, was unable to be measured because of the strong absorption tail of a phonon sideband. Taking the magnon-magnon interaction into account, the theory on temperature dependence of the magnon sideband should be reconstructed. The Raman scattering by spin wave in α-MnS is now under investigation. As it was very effective for the study of antiferromagnetic magnons in certain kinds of compounds, the experimental studies on the Raman effect will reveal different aspects of antiferromagnetism in α-MnS.

ACKNOWLEDGEMENTS

REFERENCES

1) J. W. Halley and I. Silvera: Phys. Rev. Letters 15 (1965) 654.
2) R. L. Creene et al.: Phys. Rev. Letters 15 (1965) 656.
3) K. Tsushima, K. Aoyagi and S. Sugano: J. appl. Phys. 41 (1970) 1238.
4) S. Koide and M.H.L. Pryce: Phil. Mag. 3 (1958) 607.
5) R. G. Shulman and V. Jaccarino: Phys. Rev. 108 (1957) 1219.
6) R.G. Shulman and V. Jaccarino: Phys. Rev. 109 (1958) 1084.
7) J.W. Stout: J. chem. Phys. 31 (1959) 709.
8) R. Stevenson: Phys. Rev. 152 (1966) 531.

9)   J. Owen: Disc. Farady Soc. **19** (1955) 127.

10) C.J. Ballhausen and A.D. Lier: J. molecular Spectrosc. **2** (1957) 342.

11) C.J. Ballhausen and A.D. Lier: molecular Spectrosc. **4** (1960) 190.

12) D. R. Huffman and R.L. Wild: Phys. Rev. **156** (1967) 989.

13) C.T. Anderson: J. Amer, Chem. Soc. **53** (1931) 478.

14) C. F. Squire: Phys. Rev. **56** (1939) 922.

15) H. Bizettie: Ann. Phys. (France) **1** (1946) 295.

16) J. J. Banewicz and R. Lindsay: Phys. Rev. **104** (1956) 318.

17) R. Lindsay and J.J. Banewicz: Phys. Rev. **110** (1958) 634.

18) M.E. Lines and E.D. Jones: Phys. Rev. **141** (1966) 525.

19) R.W.G. Wycoff: *Crystal Structures* (Interscience, New Yorh, 1963).

20) P. Pascal: *Nouveau Traite de Chimie Minerale* XVI (Masson et Cie, Paris, 1960) p. 949.

21) R.D. Archer and W.N. Mittchel: J. chem. Phys. **39** (1963) 250.

22) J.P. Coughlin: J. Amer. Chem. Soc. **72** (1950) 5445.

23) R. Nitsche, H.U. Bolsterli and M. Lichtensteiger: J. Phys. Chem. Solids **21** (1961) 199.

24) K. Lee: Phys. Rev. **172** (1968) 284.

25) L. Corliss, N. Elliot and J. Hastings: Phys. Rev. **104** (1956) 924.

26) D.S. Rodbell and J. Owen: J. appl. Phys. **35** (1964) 1002.

27) G. Racah: Phys. Rev. **62** (1942) 438.

28) G. Racah: Phys. Rev. **63** (1942) 367.

29) G. Racah: Phys. Rev. **76** (1949) 1352.

30) E.U. Condon and G.H. Shortley: *The Theory of Atomic Spectra* (Cambridge University Press, New York, 1953) p. 177.

31) Y. Tanabe and S. Sugano: J. Phys. Soc. Japan **9** (1954) 753.

32) Y. Tanabe and S. Sugano: J. Phys. Soc. Japan **9** (1954) 766.

33) Y. Tanabe and S. Sugano: J. Phys. Soc. Japan **11** (1956) 864.

34) J.E. Orgel: J. chem. Phys. **23** (1955) 1004.

35) J. E. Orgel: J. chem. Phys. **23** (1955) 1819.

36) J.E. Orgel: J. chem. Phys. **23** (1955) 1824.

37) R. Pappalardo: J. chem. Phys. **31** (1959) 1050.

38) R. Pappalardo: J. chem. Phys. **33** (1960) 613.

39) J.W. Stout: J. chem. Phys. **33** (1960) 303.

40) J.S. Griffith: *The Theory of Transition Metal Ions* (Cambridge University Press, Cambridge, 1961).

41) C.K. Jørgensen: Disc. Farady Soc. **57** (1961) 204.

42) J. Owen: Proc. Roy. Soc. A227 (1955) 183.

43) See, for example, C.J. Ballhausen: *Introduction to Ligand Field Theory* (McGraw-Hill, New York, 1962) p. 222.

44) K. Motizuki and I. Harada: Progr. theor. Phys. Supplement **46** (1971) 40.

45) T. Nagamiya: *Solid State Physics* ed. F. Seitz, D. Turnbull and H. Ehrenrich (Academic Press, New York, 1967) p. 305.

46) C. Kittel: *Quantum Theory of Solids* (John Willy and Sons, Inc., New York, 1963) Chap. 10, p. 213.

47) D.D. Sell, R.L. Greene and M. White: Phys. Rev. **158** (1967) 489.

48) F. Saito: Solid State Commun. **8** (1970) 969.